Electronic Supplementary Material (ESI) for New Journal of Chemistry.

A gas diffusion strategy to engineer hierarchically porous Fe-N-C electrocatalysts for the high-performance cathodes of Zn-air batteries

Yunxiao Zhang, Wenhua Xiao, Jingqiang Zhang, Tiantian Hu, Shanxia Hu, Minjie Zhou, Zhaohui Hou, Yu Liu*, Binhong He*

Key Laboratory of Hunan Province for Advanced Carbon–based Functional Materials, School of Chemistry and Chemical Engineering, Hunan Institute of Science and Technology, Yueyang 414006, Hunan, China

***Corresponding authors.**

Email addresses: hiliu2000@126.com (Y. Liu), 11990398@hnist.edu.cn (B. He)

1.1 Materials characterization

1.2 Electrochemical measurements

1.2.1 ORR performance

1.2.2 Zn–air batteries performance

Figure S1 SEM images of NCNF support.

Figure S2 (a-b) High-resolution C1s spectra and (c-d) high-resolution Fe 2p spectra of Fe–NCNF–40 and Fe–NCNF–200.

Figure S3 LSV curves at different rotating speeds for (a) Fe–NCNF–40, (c) Fe–NCNF–120, and (e) Fe–NCNF–200 in O_2-saturated 0.1 M KOH electrolyte (scan rate: 10 mV s^{-1}). K-L plots at various potential for (b) Fe–NCNF–40, (d) Fe–NCNF–120, and (f) Fe–NCNF–200 in O_2-saturated 0.1 M KOH electrolyte.

Table S1 The specific BET result of Fe–NCNF–40, Fe–NCNF–120, and Fe–NCNF–200.

Table S2 The XPS result of Fe–NCNF–40, Fe–NCNF–120, and Fe–NCNF–200.

Table S3 The N 1s spectra fitting result of Fe–NCNF–40, Fe–NCNF–120, and Fe–NCNF–200.

Table S4 The Fe contents in the prepared catalysts obtained from ICP-OES.

Table S5 A comparison table of the ORR performance between this work and recently reported Fe-N-C catalysts in 0.1 M KOH solution.

1.1 Materials characterization

The surface morphologies of the resulting samples were examined by scanning electron microscopy (SEM, JEOL, JSM-6630f) and transmission electron microscopy

(TEM, JEOL, JEM-2100). The crystal structure and defect properties of the samples were characterized by x-ray diffraction (XRD, Rigaku, Ultima IV) and Raman spectroscopy (WITec alpha300R). X-ray photoelectron spectroscopy (XPS) measurements are used to analyze the surface and chemical composition of the sample with a Thermo Scientific K-Alpha. The specific surface area (SSA) and pore distribution of the samples were measured using a microscopic analyzer (ASAP2020HD) by recording N_2 adsorption/desorption isotherms.

1.2 Electrochemical measurements

1.2.1 ORR performance

The electrochemical activity of the sample was measured for ORR performance using a CHI 760E electrochemical workstation in a standard three-electrode system with a platinum foil and saturated Ag/AgCl electrode as counter electrode and reference electrode, and a 5 mm diameter rotating disk electrode (RDE) loaded with catalysts as the working electrode. 4 mg of catalysts were dispersed in 980 μL of ethanol and 20 μL of 5 *wt*% Nafion solution to make the catalyst ink. After 30 minutes of sonication, 20 μL of catalyst ink was spread onto the RDE and naturally dried at room temperature. The geometrical surface area of the disc electrode is 0.196 cm^2 and the catalyst loading is 0.4 mg cm^{-2}. For comparison, commercial Pt/C catalyst (De Nora Elettrodi Co. Ltd., 20 *wt*.% Pt on carbon black) with the same loading amount is studied under the same circumstances.

The ORR activities of catalysts were detected in O_2-saturated 0.1 M KOH solution by using a rotating disk electrode (Pine Instrument, MSR analytical rotator).

The ORR kinetic parameters were analyzed by the following Koutechy Levich (K-L) equation:

$$\frac{1}{J}=\frac{1}{0.62nFC_0D_0^{2/3}\nu^{-1/6}\omega^{1/2}}+\frac{1}{J_k}$$

Where J is the tested current density, J_K means kinetic current density. n represents the electron transfer number, F refers to Faraday constant (96485 C mol^{-1}), C_0 is oxygen bulk concentration (1.2×10^{-3} M in 0.1 M KOH), D_0 is the oxygen diffusion coefficient (1.9×10^{-5} cm^2 s^{-1} in 0.1 M KOH), v is electrolyte kinetic viscosity (0.01 cm^2 s^{-1}) and ω is disk angular velocity.

In basic electrolyte (0.1 M KOH), all potentials can be converted to reversible hydrogen electrode (RHE) by the following equation: $E_{RHE}=E_{Ag/AgCl}$ + 0.97 V. Cyclic voltammetry (CV) curve was tested in N_2 or O_2 saturated electrolyte within a voltage range from -0.2 to 1.2 V (*vs*. RHE) at a scan rate of 50 mV s^{-1}. Linear sweep voltammetry (LSV) curve was measured at a scan rate of 10 mV s^{-1} at various rotation speeds from 400 to 1600 rpm within identical voltage range. The onset potential is determined by making a tangent line to the horizontal line and a tangent line to the descending slope, intersecting at a point at which the corresponding potential is the onset potential.

1.2.2 Zn-air batteries performance

In handmade electrochemical cells, tests on liquid Zn–air batteries (ZAB) were carried out. The air cathode is made of hydrophobic carbon paper (3 cm * 3 cm) with a gas diffusion layer on the air-facing side and a catalyst layer on the water-facing side. The loading amount for for NCNF–1 or Pt/C catalyst (20 *wt*.% Pt on carbon

black) is 0.9 mg cm^{-2} onto carbon paper, warping the current collector (copper-foam). As the anode, a polished Zn plate (3 cm * 8 cm) was used. The electrolyte for ZAB is 6 M KOH containing 0.2 M $Zn(Ac)_2$. ZAB was performed with a homemade zinc-air battery and the CHI 760E electrochemical workstation and LAND.

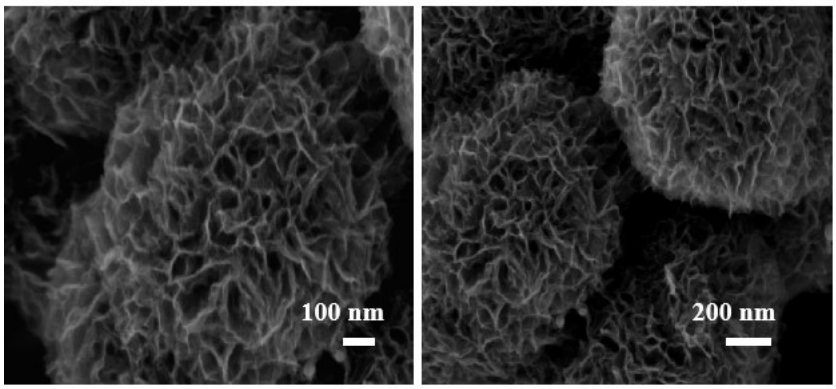

Figure S1 SEM images of NCNF support.

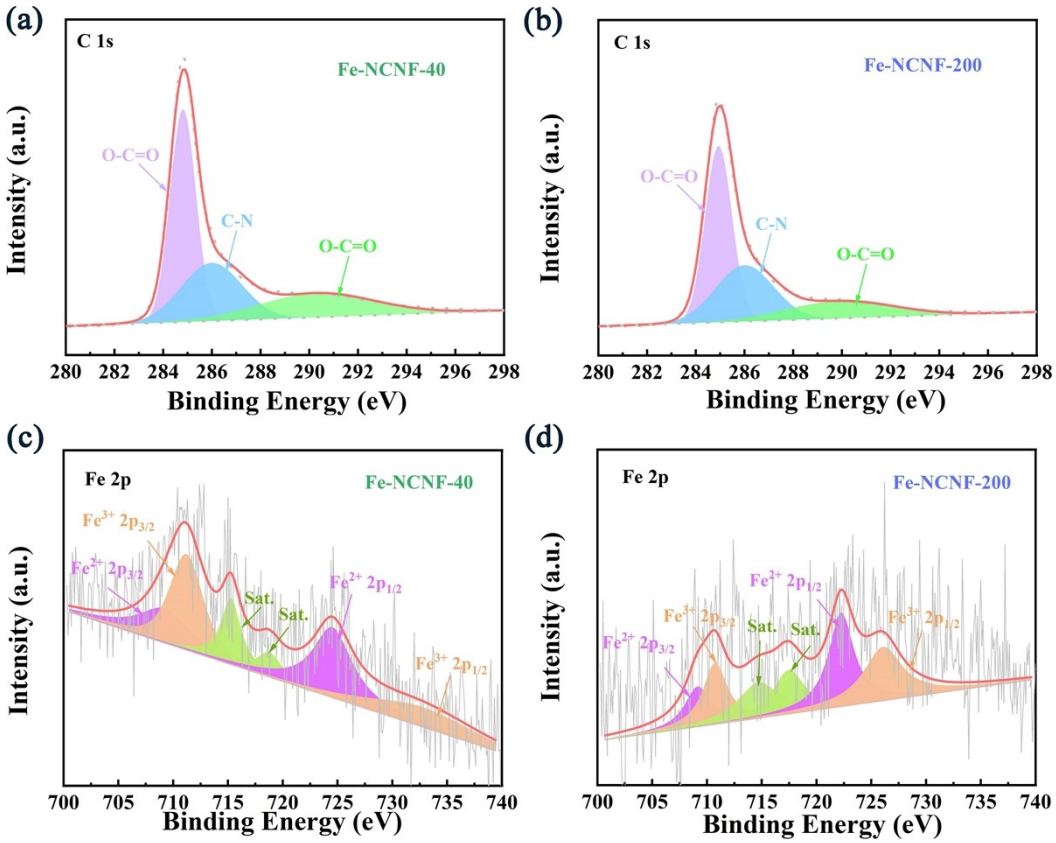

Figure S2 (a-b) High-resolution C1s spectra and (c-d) high-resolution Fe 2p spectra of

Fe–NCNF–40 and Fe–NCNF–200.

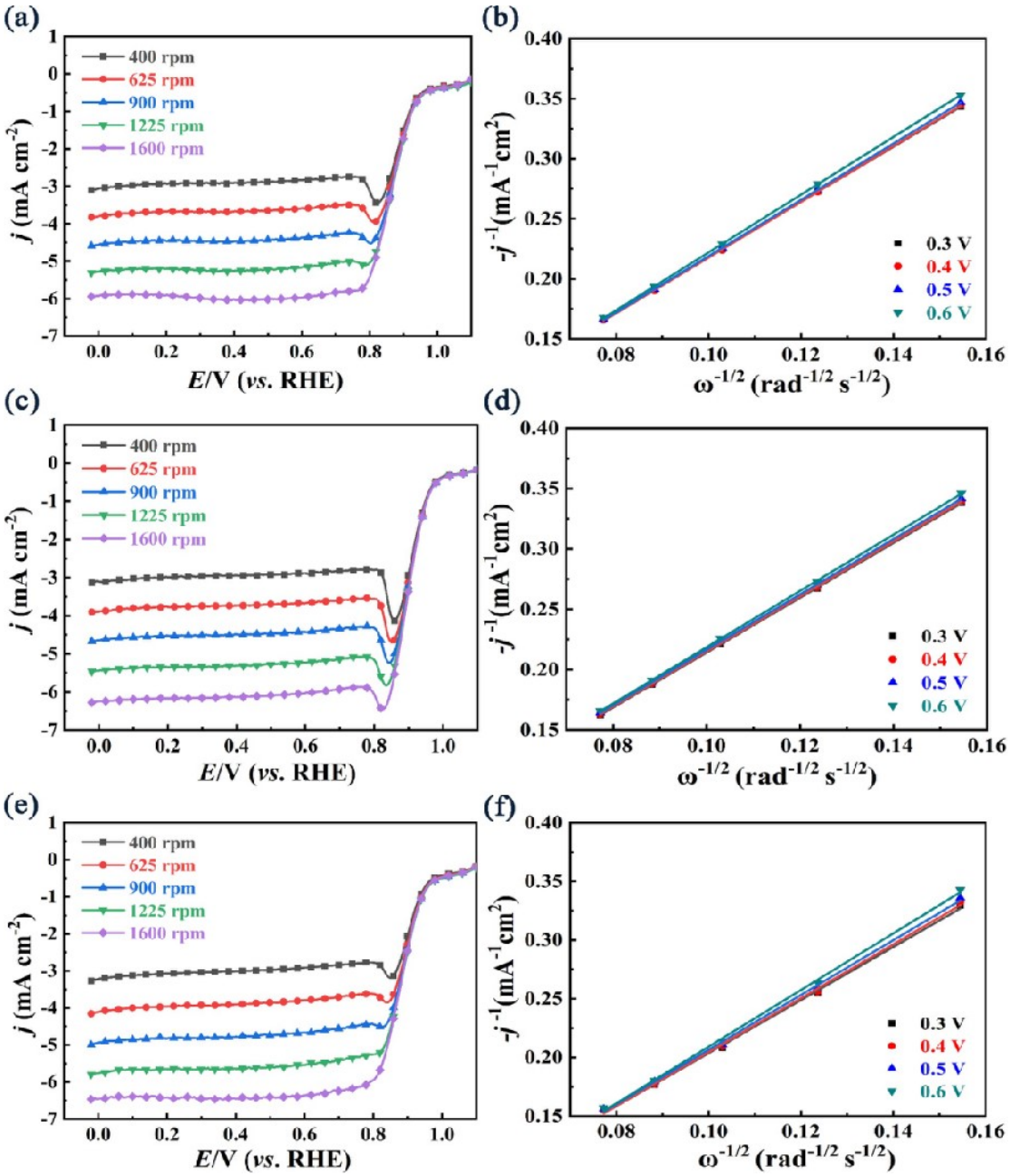

Figure S3 LSV curves at different rotating speeds for (a) Fe–NCNF–40, (c) Fe–NCNF–120, and (e) Fe–NCNF–200 in O_2-saturated 0.1 M KOH electrolyte (scan rate: 10 mV s^{-1}). K-L plots at various potential for (b) Fe–NCNF–40, (d) Fe–NCNF–120, and (f) Fe–NCNF–200 in O_2-saturated 0.1 M KOH electrolyte.

Table S1 The specific BET result of Fe–NCNF–40, Fe–NCNF–120, and Fe–NCNF–200.

Samples	Specific Surface Area (m^2 g^{-1})	Pore Volume (cm^3 g^{-1})	Pore size (nm)
Fe–NCNF–40	1004.93	0.81	8.29
Fe–NCNF–120	946.91	1.33	11.45
Fe–NCNF–200	939.16	1.16	12.16

Table S2 The XPS result of Fe–NCNF–40, Fe–NCNF–120, and Fe–NCNF–200.

Samples	C (at. %)	N (at. %)	O (at. %)	Fe (at. %)
Fe–NCNF–40	93.90	2.36	3.63	0.11
Fe–NCNF–120	93.48	2.10	4.21	0.21
Fe–NCNF–200	89.91	2.06	7.67	0.36

Table S3 The N 1s spectra fitting result of Fe–NCNF–40, Fe–NCNF–120, and Fe–NCNF–200.

Samples	Pyridinic-N (Fe-N) (%)	Pyrrolic–N (%)	Graphitic–N (%)	Oxygenated–N (%)
Fe–NCNF–40	16.51	24.09	46.20	13.20
Fe–NCNF–120	21.37	17.27	47.50	13.86
Fe–NCNF–200	18.19	19.16	48.53	14.10

Table S4 The Fe contents in the prepared catalysts obtained from ICP-OES.

Samples	Fe (wt%)
Fe–NCNF–40	0.28
Fe–NCNF–120	0.48
Fe–NCNF–200	0.69

Table S5 A comparison table of the ORR performance between this work and recently reported Fe-N-C catalysts in 0.1 M KOH solution.

Materials	$E_{1/2}$ (V) (vs. RHE) in 0.1 M KOH	References
Fe–NCNF–120	0.90	This work
Fe-N-c	0.82	[1]
FeNC	0.86	[2]
FeSA/HNPC	0.84	[3]
Fe–N–Cwood	0.84	[5]
FNG	0.90	[6]
Hemin@C_3N_4-900Zn	0.89	[7]
(Fe-N-C/HPCS@CNT	0.87	[8]
Fe_3O_4/Fe_3N/Fe-N-C@PC-2.5	0.87	[9]
Fe-PA/ML0.5-900	0.90	[10]
CA-Fe/MF-N900	0.86	[11]

References

[R1]Chanez M,Yazhou Z,Bing L, et al. A Stabilized Assisted Method for the Synthesis of Fe-N-C Catalysts for the Oxygen Reduction Reaction[J]. Journal of The Electrochemical Society,2022,169(6).

[R2]Williane F S D,Pablo P P M,Alessandra D, et al. Nanostructured Fe-N-C as Bifunctional Catalysts for Oxygen Reduction and Hydrogen Evolution[J]. Catalysts,2021,11(12).

[R3]Xinxin J,Yan X,Junhong F, et al. A Highly Efficient Fe−N−C Electrocatalyst with Atomically Dispersed FeN4 Sites for the Oxygen Reduction Reaction[J]. ChemCatChem,2021,13(11).

[R4]Dingding L,Zheng H,Kunyue L, et al. Biomass wood-derived efficient Fe–N–C catalysts for oxygen reduction reaction[J]. Journal of Materials Science,2021,56(22).

[R5]Ailing S,Hao T,Wang Y, et al. Enhanced confinement synthesis of atomically dispersed Fe-N-C catalyst from resin polymer for oxygen reduction[J]. Journal of Energy Chemistry,2022,65.

[R6]Zhaoxu L,Xinyi L,Meifang L, et al. Molecule-confined modification of graphitic C_3N_4 to design mesopore-dominated Fe-N-C hybrid electrocatalyst for oxygen reduction reaction[J]. International Journal of Hydrogen Energy,2021,46(59).

[R7]Fei F,Haoran Z,Rui Y, et al. Anchoring Fe-N-C Sites on Hierarchically Porous Carbon Sphere and CNT Interpenetrated Nanostructures as Efficient Cathodes for Zinc-Air Batteries.[J]. ACS applied materials & interfaces,2021.

[R8]Hao R,Chen J,Wang Z, et al. Iron polyphthalocyanine-derived ternary-balanced Fe_3O_4/Fe_3N/Fe-N-

C@PC as a high-performance electrocatalyst for the oxygen reduction reaction[J]. Science China Materials,2021,64(12).
[R9]Azhar M,Nanhong X,Bolin Z, et al. Optimizing Surface N-Doping of Fe-N-C Catalysts Derived from Fe/Melamine-Decorated Polyaniline for Oxygen Reduction Electrocatalysis[J]. Advanced Materials Interfaces,2021,8(13).
[R10]Liu J,Zhu Y,Fan C, et al. Three-Dimensional Porous Fe–N–C Derived from Iron-Citrate-Functionalized Melamine Foam as a Highly Active Oxygen Reduction Catalyst for Zn–Air Batteries[J]. Energy Technology,2020,8(6).